# *Biocompatible Alginate Microgel Particles as Heteronucleants and Encapsulating Vehicles for Hydrophilic and Hydrophobic Drugs*

# Biocompatible Alginate Microgel Particles as Heteronucleants and Encapsulating Vehicles for Hydrophilic and Hydrophobic Drugs

*Huseyin Burak Eral‡, Vilmalí López-Mejías‡, Marcus O'Mahony, Bernhard L. Trout, Allan S. Myerson and Patrick S. Doyle**

Novartis-MIT Center for Continuous Manufacturing and the Department of Chemical Engineering, Massachusetts Institute of Technology, 77 Massachusetts Avenue, E19-502b, Cambridge, MA 02139.

ABSTRACT: Biocompatible materials that can control crystallization while carrying large amounts of active pharmaceutical ingredients (APIs) with diverse chemical properties are in demand in industrial practice. In this study, we investigate the utility of biocompatible alginate (ALG) hydrogels as a rational material for crystallizing and encapsulating model APIs that present drastically different solubilities in water. Acetaminophen (ACM) and fenofibrate (FEN) are utilized as the model hydrophilic and hydrophobic moieties, respectively. ALG hydrogels with different ALG concentrations (hence different mesh sizes) are utilized as heteronucleants to control the nucleation kinetics of ACM from solution. ALG hydrogels with smaller mesh sizes showed faster nucleation kinetics. We hypothesize that this behavior is due to the interplay between the polymer-solute interactions and the mesh-induced confinement effects. The loading

of ACM into hydrogels by equilibrium partitioning is quantified and found to be inversely proportional to ALG concentration. For hydrophobic model APIs, loading via equilibrium partitioning is inefficient; hence we suggest emulsion-laden hydrogels where emulsion droplets are encapsulated inside the hydrogel matrix. The incorporation of emulsion droplets inside hydrogels enables the high loading of the hydrophobic API leveraging the high solubility of the hydrophobic API in the dispersed emulsion droplets. By carefully choosing the emulsification method and the dispersed phase, we demonstrate significant loading (up to ~80% w/w) and crystallization of the stable form of FEN. Our results provide new insights for designing biocompatible nucleation-active materials capable of carrying industrially significant amounts of water-soluble and insoluble APIs in the crystalline form and serving as designer final drug formulation.

**Introduction**

Crystallization is omnipresent in nature and industrial practice, and is of particular significance to the chemical and pharmaceutical industry[1, 2]. It is notoriously difficult to control and scale up as a significant portion of the crystallization process starts at foreign interfaces such as container walls, impurities and dust. A promising direction for controlling crystallization is to target nucleation, a critical step in the process, by designing heteronucleant materials capable of influencing crystallization through selective interactions. However, in industrial practice, particularly in the pharmaceutical industry, compounds to be crystallized are diverse in chemical structure and hence in physical properties such as solubility. Therefore the heteronucleant materials in industrial practice should be biocompatible, capable of controlling crystallization while carrying industrially relevant amounts of both hydrophobic and hydrophilic compounds in crystalline form.

Controlling nucleation of active pharmaceutical ingredients (APIs) with heteronucleants remains challenging due not only to the diverse chemical nature of APIs but also due to the sensitivity of the nucleation barrier to experimental conditions[3] and the physical properties of the interface inducing nucleation[4, 5]. Although many attempts have been made to control nucleation by gaining understanding of the experimental conditions, the scarcity of investigations studying the role that interfacial properties play during nucleation may hinder our capacity to rationally design heteronucleants, to this end, this paper aims to provide new insights for designing biocompatible nucleation-active materials capable of carrying industrially relevant quantities of water-soluble and insoluble APIs in the crystalline form.

Considerable progress has been made in understanding the role of interfaces on nucleation. Among the proposed mechanism, epitaxy and functional group chemistry has been successful in describing nuclei formation on surfaces such as self-assembled monolayers[6-9], molecular single-crystal surfaces[10] and crystalline polymer surfaces[5]. Interfaces can influence nucleation via polarization matching in cases where both the interface and the crystal exhibit a net dipole interaction[11, 12] as well. Furthermore, the geometry and the porosity of the interface at length scales relevant to nucleation are shown to affect not only nucleation kinetics[13, 14] but also polymorphism[15-17]. Despite the considerable strides made with the aforementioned crystalline interfaces, their material properties are not easily adjustable. Non-crystalline materials such as hydrogels offer a more promising option as their structure, topology, interfacial and mechanical properties can be easily tuned with a wide range of fabrication methods. In particular, synthetic poly(ethylglycol) (PEG) hydrogels with tunable microstructures have been demonstrated to be exceptional materials for controlling nucleation kinetics of hydrophilic APIs[18-20]. The hydrogels influence nucleation kinetics through two distinct mechanisms, confinement[21-25] and favorable

solute-polymer interactions[26]. In contrast to rigid nanoporous materials previously reported for studying nucleation under confinement[15, 16, 27], soft polymer gels are solvated. Therefore, they can swell and concentrate solute molecules within the polymer network via thermodynamic partitioning driven by favorable polymer−solute interactions.

Despite their ease of fabrication and utility as model hydrogels, previously evoked PEG hydrogels are prepared by free radical polymerization[26], a process strongly avoided in the pharmaceutical industry. In an effort to create pharmaceutically acceptable nucleation active hydrogels capable of carrying APIs of distinct water solubilities, we turn to alginate (ALG), a biocompatible polysaccharide widely used in the food and pharmaceutical industry [28-32]. ALG - isolated from brown algea- is a linear copolymer, consisted of b-D-mannuronic acid (M) and its C-5 epimer, a-L-guluronic acid (G), arranged in a block-wise pattern. Gel formation can be induced by lowering pH or by adding various divalent cations, in particular $Ca^{2+}$, which crosslinks a pair of G blocks within the alginate chains. Despite its utility for carrying hydrophilic drugs[33], ALG is hydrophilic in nature hence it cannot be loaded with significant amounts of hydrophobic drugs [32].

It is important to note that a significant fraction of pharmaceuticals are of hydrophobic nature and do not lend themselves effectively to thermodynamic partitioning[34]. Considerable efforts have been placed on synthesizing/modifying hydrogels capable of carrying hydrophobic moieties[35, 36]. For instance, hydrogels can be modified by co-polymerizing or grafting hydrophobic units to hydrophilic polymer network effectively creating hydrophobic meso-scale regions[37]. Nevertheless, these methods are not effective for loading high weight percentages of APIs into the hydrogel. Recently, emulsion-laden hydrogels containing nano-[38] and microemulsions[39, 40] have been used for delivery\controlled release of model hydrophobic

cargo[41-43]. However, the focus of these studies has been on controlled release not on crystallization.

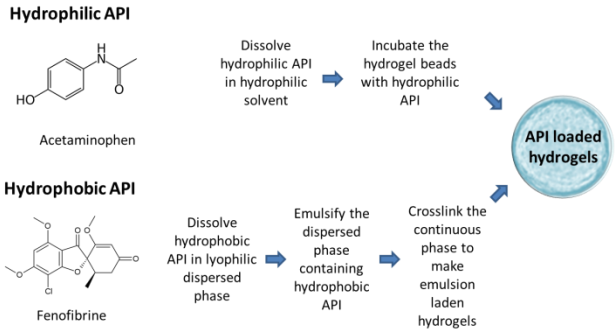


**Figure 1.** Illustration of the two routes developed for formulating hydrophobic and hydrophilic API loaded hydrogels

In an effort to develop a biocompatible material capable of controlling crystallization and carrying large amounts of the APIs of diverse chemical nature, we investigate the utility of ALG hydrogels as heteronucleants and encapsulation vehicles to carry APIs in crystalline form (Figure 1). For model hydrophilic APIs, we investigate ALG hydrogels with different mesh sizes. For hydrophobic APIs, we developed emulsion-laden hydrogels leveraging the ability of lyophilic emulsion droplets to dissolve and carry large amounts of hydrophobic APIs. We investigate ALG hydrogels as heteronucleants for the model hydrophilic API (Acetaminophen, ACM), the mesh size ($\xi$) of the hydrogel network is systematically varied by manipulating the polymer concentration. ACM nucleation kinetics from solution and ability of encapsulation of the API into the hydrogel through equilibrium partitioning are quantified as a function of mesh size. We demonstrate that emulsion-laden hydrogels can carry large amounts of fenofibrate (FEN) and can crystallize the stable form of FEN. Through careful choice of the dispersed phase and emulsification methods, we developed optimal formulations of emulsion-laden ALG hydrogels

that are capable of carrying adjustable and industrially relevant amounts (up to 80% w/w) of FEN in crystalline form.

## Methods and Materials:

***Materials:*** Sodium alginate (Na-ALG) isolated from brown algae is purchased from Sigma Aldrich (CAS# 9005-38-3). The weight average molecular mass is between 80,000 - 120,000. The mannuronic acid and guluronic acid ratio is 1.56. Compounds $CaCO_3$ (mean particle size 10 μm, CAS # 471-34-1), Sodium Chlorine (NaCl, CAS# 7647-14-5), 4-(2-Hydroxyethyl)piperazine-1-ethanesulfonic acid, N-(2-Hydroxyethyl)piperazine-N′-(2-ethanesulfonic acid) (Hepes, CAS# 7365-45-9) and glucono-δ-lactone (GDL, CAS# 90-80-2) are purchased from Sigma-Aldrich. Acetaminophen (ACM, CAS# 103-90-2) and Fenofibrate (FEN, CAS# 49562-28-9) are purchased from Sigma-Aldrich.

***Preparation of Na-alginate solutions:*** Na-Alginate solutions are prepared by dissolving the polysaccharide powder in aqueous deionized water with NaCl 0.3M, Hepes 20 mM (pH 7.4) at final ALG concentrations of 2, 4, 6, 8, 10, and 12 w/v %. The homogeneity of solution is assured by rigorous magnetic stirring[44].

***Preparation of Crystallization solutions for induction time measurements:*** The ACM crystallization solution is prepared by dissolving ACM powder (10g) in 50 mL of ethanol at 65°C. The FEN crystallization solutions are prepared by dissolving powdered FEN (450 mg and 15 g) in heptane (50 mL) and ethyl acetate (25 mL) at 65°C.

***Preparation of disk shaped ALG hydrogels for rheological measurements:*** For rheological measurements, $Ca^{+2}$ saturated disk shaped hydrogels are prepared by two stage crosslinking. In

the first stage, Na-ALG solutions are mixed by an inactivated form of $Ca^{+2}$ ($CaCO_3$, 20 mM) followed by the addition of the slowly hydrolyzing glucono-δ-lactone (GDL), maintaining a ratio $[GDL]/[Ca^{+2}] = 2$. The suspension is degassed prior to the addition of GDL to avoid bubble formation. Removing bubbles entrapped in Na-ALG solution for high weight Na-alginate solutions is required to get clean measurements. The hydrogels are cured in a Petri dish (35 mm diameter) for 24 h to get cylindrically shaped hydrogels. In the second phase of curing, three milliliters of a 6% w/v aqueous $CaCl_2$ added to hydrogels from previous crosslinking step. The hydrogels are cured for 48 h prior to rheological measurement ensuring that $Ca^{2+}$ saturates all the possible binding sites. The final dimensions of the hydrogels used for rheological determination are 3 mm height and 20 mm in diameter.

***Preparation of spherical ALG hydrogel beads:*** Na-ALG solutions prepared as reported are dripped into a gelling bath containing 6% w/v $CaCl_2$. The ALG gel beads are aged for 24 h in the gelling solution prior to analysis. The average diameter of the beads is 750 μm (COV Coefficient of variation: 8%).

***Rheological Measurements:*** Rheological characterization of disk shaped ALG hydrogels is performed with controlled stress rheometer TA 2000 with a plate and plate geometry (20 mm) and operating at 20 °C. To avoid evaporation, the measurements are performed with a solvent trap. Sand paper is used to eliminate wall slip. To identify the optimum gap height that eliminates the wall slip and the excessive gel squeezing (reflecting in the alterations of polymeric network properties), the gap is reduced systematically while executing a series of short frequency sweeps with strain = 0.05%. The selected gap maximizing the value of the elastic modulus G' is reported. We also ensured that the normal force applied on samples prior to measurement does not exist 1 N for each measurement. For each hydrogel of a given weight fraction, the linear

viscoelastic range is identified by a stain sweep with increasing strain stress ($0.01\% < \gamma < 1000\%$) with frequency ($\omega$) 20 rad/s. The stain chosen to perform the frequency sweep is an order of magnitude lower than yield stain of the weakest gel. The frequency sweeps are performed at 0.05% strain that is two orders of magnitude lower than the yield stress. All tests (stress and frequency sweep) are performed in triplicate.

***Procedure for synthesizing emulsion-laden hydrogels:*** The procedure for synthesizing emulsion laden hydrogel capable of carrying hydrophobic API can be divided into three steps (i) dissolving the API in dispersed phase, (ii) emulsifying the API carrying dispersed phase in continuous phase containing the ALG biopolymer, (iii) crosslinking ALG to capsulate emulsion-laden hydrogel beads (Figure 1).

**Emulsification for preparing emulsion-laden hydrogels**

***Magnetic stirring:*** In magnetic stirring emulsification, the dispersed phase with dissolved API is slowly dripped into the continuous phase containing surfactant in 100 mL flask as a magnetic stirrer emulsifies the dispersed phase droplets at 1000 rpm. For all the formulations, a 1% by volume Pluronic® F-68 (polyoxyethylene(PEO)-polyoxypropylene(PPO) block copolymer) purchased from Sigma Aldrich is used. The volume fraction of the dispersed oil phase is set by adjusting the volume of dispersed phase dripped into the flask relative to the volume of continuous phase containing 2% w/v ALG.

***High Pressure homogenization:*** In high pressure homogenization (HPH), a pre-emulsion solution prepared by magnetic stirring is emulsified by pumping the solution through a homogenization valve that varies its diameter with respect to the applied pressure. The applied pressure can be varied to achieve pressure drops between 5 to 25 kpsi across homogenization

valve that directly influences the size and polydispersity of emulsified droplets[38]. For the emulsions utilized in this study, High HPH of the pre-emulsion is carried out using an Avestin Emulsiflex-C3 homogenizer operating at 15 kpsi. Number of passes is set to N=10.

***Method of crosslinking Na-ALG containing emulsions:*** Na-Alginate solutions containing emulsion at desired volume fraction are dripped into a gelling bath containing 6% w/v $CaCl_2$. The ALG concentration is defined as the concentration in the continuous phase and all the samples prepared it is set to 4% w/v. The ALG gel beads are aged for 24 h in the gelling solution prior to analysis to completely crosslink Na-ALG.

***Characterization of emulsions and emulsion-laden hydrogels:*** The size of emulsion droplets prepared by magnetic stirring is characterized by inverted microscope (Axiovert 200, Zeiss). Nanoemulsion droplet sizes are measured via dynamic light scattering using a Brookhaven Instruments BI-200SM multi-angle apparatus. Samples are diluted to $\varphi = 0.0005$ in deionized water. Autocorrelation functions are measured at a scattering angle of 90° and a temperature of 25°C. Cumulant analysis is conducted on the data acquired to obtain the hydrodynamic droplet diameter distribution. Coefficient of variation (COV) is defined here as the variance of the size distribution relative to the mean size. We visualized the emulsion-laden hydrogels by environmental scanning tunneling microscope (ESEM) FEI/Philips XL30 in hydrated form. Scanning electron microscopy (JEOL 5910 General Purpose SEM) is used to analyze the surfaces of dried particles.

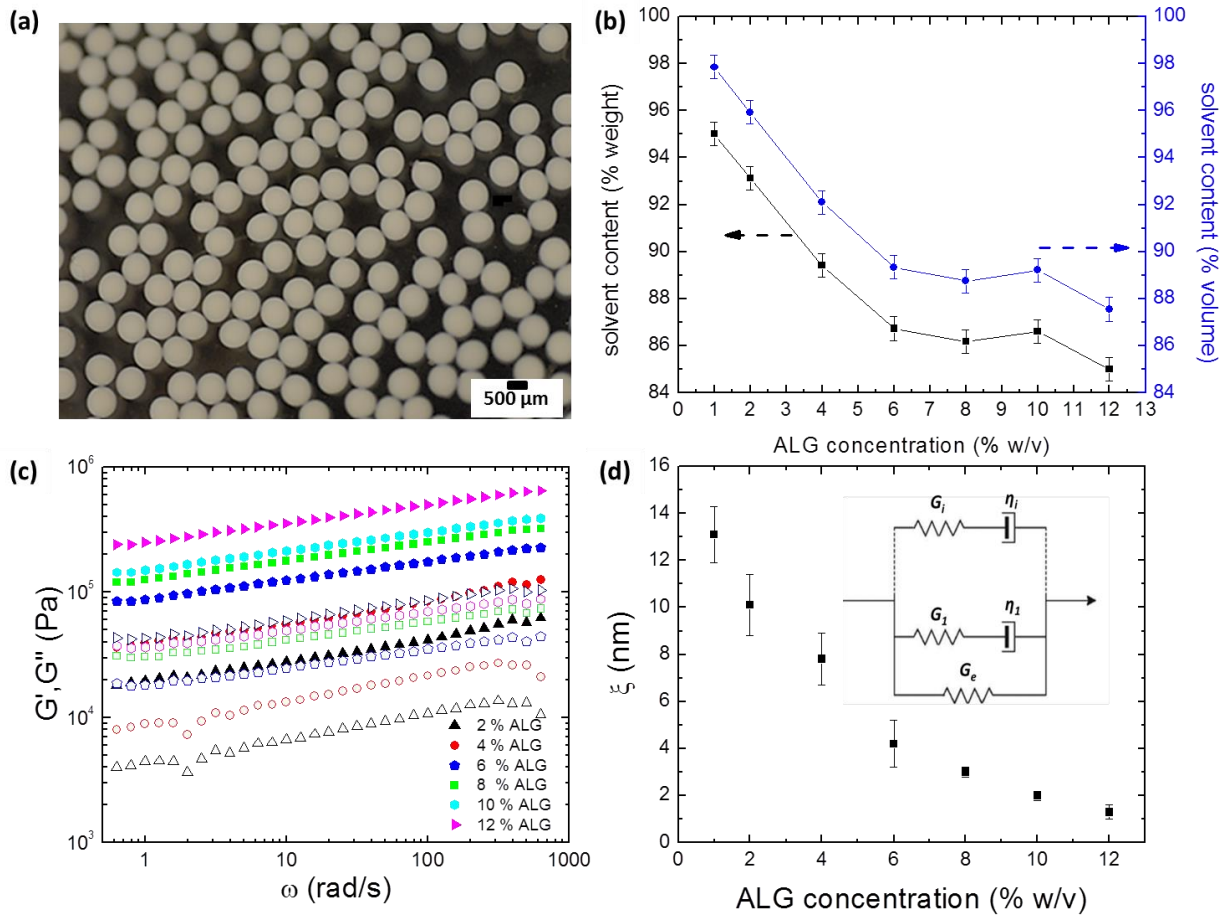


**Figure 2.** (a) Optical micrographs of 4 %w/v ALG hydrogel beads with mean size 760 µm with standard deviation 52 µm (coefficient of variation: 0.08). (b) The solvent content by weight (left hand axis) and by volume (right hand axis) calculated from evaporation experiments. (c) Rheological measurements for ALG hydrogels prepared with different Na-ALG concentrations. (d) The average mesh size and mechanical illustration of Maxwell model for calculating mesh size (inset).

## Characterization of ALG Hydrogels:

We characterized ALG hydrogels in terms of solvent content and mesh size: (i) the solvent content is quantified by evaporation measurements and (ii) the mesh size is characterized by rheological measurements. Both methods are described in detail in The Materials and Methods

section. For the evaporation measurements spherical ALG beads (Figure 2a) are used whereas for rheological measurements disk-shaped hydrogels are prepared due to the requirements of the rheometer. It is important to note that both hydrogel geometries are $Ca^{+2}$-saturated to completely crosslink ALG hydrogels. The evaporation measurements provided information on the weight ratio of the solvent to the hydrogel beads, which is then converted to a volume ratio of hydrogel as the volume of the bead is known *a priori*. The hydrogel beads (approximately 20 beads) are first pat dried, and weighed and then an optical image is taken to estimate the size (Figure 2a). The beads are placed in a vacuum oven 120 °C over-night to evaporate the solvent. The weight change between the hydrated and dried hydrogel is recorded as the weight of the evaporated solvent. The weight of the evaporated solvent is converted to the volume evaporated, as the density of the solvent is known. The weight and the volume ratio of the solvent to the ALG are given in Figure 2b. All the measurements are performed in triplicate.

The characterization of mesh size for ALG hydrogels with different ALG concentrations is performed by oscillatory rheology. The disk-shaped ALG gels at different ALG concentrations, namely, 2, 4, 6, 8, 10 and 12% (w/v), are prepared in calcium-saturated conditions and their rheological response are recorded (Figure 2c). In all ALG concentrations considered, the storage (G') modulus is monotonous and significantly higher than the loss modulus (G''), indicating strong gel behavior. Frequency sweep measurements at a fixed strain (0.05%) are modeled in terms of the generalized Maxwell model[45]. The model utilized is composed of a sequence of elements in parallel (spring and dashpot) to which an additional spring has been added (Figure 2d and Supporting Information). The use of the generalized Maxwell model and rubberlike elasticity theory allows determination of the shear modulus, G and average mesh size ($\xi$).

As the mechanical characterization performed in the linear viscoelastic region, the response of the ALG network is dominated by entropic contribution[46]. The average mesh size can be estimated as $\xi = \sqrt[3]{\frac{6\alpha RT}{\pi N_A G}}$ from the shear modulus G where $N_A$ is the Avogadro's number, T is temperature, α is a dimensionless constant.

To estimate the prefactor, α, we turn to previous work performed in low-weight-fraction ALG gels where mesh size is determined via various techniques and compared to rheological characterization[44]. In the work of Turco *et al* [44], α is estimated to be 16.1 by comparing the rheological, TEM and NMR measurements for ALG concentrations less than 4%. We expect that that this front factor applies to our measurements with higher ALG concentrations as the front factor accounts for the deviations from point-like, compressible crosslinks of ideal rubber as described in the Flory Theory[47]. Furthermore, the mesh size values calculated agree well with the previously reported values at lower ALG concentrations[48] (Supporting Information).

**Measuring the partitioning coefficient of hydrophilic API:** Prior to insertion into the saturated solution (200mg/mL ACM in ethanol at 27°C), the hydrogel beads previously immersed in ethanol are pat-dried, weighed and imaged for size determination. The beads are left to equilibrate over three days to ensure the equilibrium partitioning of API between the continuous phase and the hydrogel. The hydrogels are later pat-dried, weighed and imaged again. The difference in weight before and after the equilibration is attributed to the API in the hydrogel. Since the mass of API in hydrogels, average diameter of beads and the number of beads is known, the concentration of API is calculated ($C_{API\ in\ hydrogel}$). The concentration of API in continuous phase ethanol ($C_{API\ in\ ethanol}$) is calculated as the initial mass of API in ethanol minus

the mass of API in the hydrogels divided by the initial volume of ethanol. The partitioning coefficient is calculated as the ratio of two concentrations $\kappa = \frac{C_{API\ in\ hydrogel}}{C_{API\ in\ ethanol}}$ given in Figure 3a. We observed similar results when we measured the partitioning coefficient using the remaining amount of ACM in solvent.

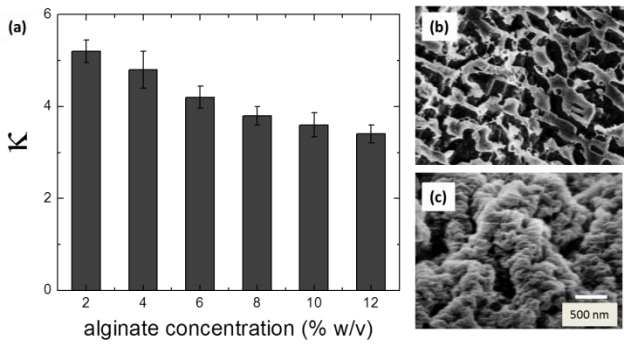


**Figure 3.** (a) Partition coefficient of ACM for different ALG concentrations. (b) Cross section of a 4 w\v% ALG bead first pat-dried, then dried in an oven at 120 °C overnight prior to SEM imaging and (c) cross section of a 4 w\v% ALG bead loaded with ACM.

**Procedure for dissolution profile of hydrophobic API in the emulsion-laden hydrogels:** The release kinetics of FEN from the emulsion-hydrogels was carried out at 37 °C while the solution is stirred at 75rpm. The dissolution medium was prepared by adding 0.72% w/v SDS to aqueous media at pH 6.8[49]. Three samples of 2 mL were taken from the 600 ml vessel at each time point and UV absorption were recorded as a function of time. The total amount of dried emulsion-laden hydrogels prepared with EA as dispersed phase was 250 mg. The solvent EA was evaporated at 50 °C overnight.

**Procedure for measuring loading of hydrophobic API in the emulsion-laden hydrogels:** For hydrophobic drugs, the dispersed phase is emulsified in nano- and micron- size droplets using

heptane and ethyl acetate as solvent to load the drugs inside the ALG particles (Figure 7a). The emulsified solution is added to the ALG solution of various concentrations and these are cross-linked *in situ* in a calcium chloride solution. The emulsion-laden hydrogels are synthesized with different emulsion volume fractions ranging from 10 to 50%. For each measurement of a given volume fraction (φ), two batches of emulsion-laden hydrogels are prepared with the same method of emulsification followed by crosslinking: preparing a reference batch without API and a test batch with API. Both batches containing approximately 200 mg of ALG beads are pat-dried and weighed. The samples containing both batches are placed in a vacuum oven and dried over two days above the boiling point of dispersed phase at 140 °C (boiling point of heptane 98 °C, ethyl acetate 77.1 °C at 1 bar). Initially heptane was used as the continuous phase; later in an effort to maximize the loading, ethyl acetate was used. The solubility of FEN in ethyl acetate is considerably larger than in heptane (9 mg/mL and 600 mg/mL). Loading is defined as the difference in weight between the hydrogels containing the API-carrying emulsions and control batch the without the API divided by weight of the API-carrying emulsion laden hydrogel on dry solute basis as: $Loading\ \% = \frac{W_{API\ carrying\ emulsion\ laden\ hydrogel} - W_{reference\ emulsion\ laden\ hydrogel}}{W_{API\ carrying\ emulsion\ laden\ hydrogel}} * 100$. To estimate the variation in loading and significance of variation, we repeated loading measurements in ten replicates. ESEM images confirm the presence of the emulsified droplets inside the ALG particle (Figure 7b-c). Additionally, TGA analysis showed that when hydrophobic drugs are encapsulated through HPH or magnetic stirrer emulsification, the residual solvent content is less than the method utilized for hydrophilic drugs (Supporting Information).

**Results and Discussion:**

We investigate ALG hydrogels as heteronucleants, and to encapsulate crystalline materials. To investigate the potential use of ALG hydrogels to influence nucleation, ALG particles of different concentrations and, hence mesh size are utilized as heteronucleants during crystallization from solution. ACM was crystallized using ethanol as a solvent (Figure 4). The crystallization solution (200 mg/mL) is undersaturated at room temperature and saturated (S = 1.5x) at 10ºC. Seventy-eight vials are prepared in total. The effect on crystal nucleation of five ALG concentrations, -4, 6, 8, 10 and 12%- are investigated using thirteen vials for each concentration. Each 1 mL vial contained 4-8 ALG particles of a particular concentration. About 750μL of the crystallization solution is delivered to each vial. Additionally, 13 vials that did not contain any ALG particles are prepared as controls. The samples were crash cooled from 65°C to 10°C to achieve a 1.5x supersaturated solution. The heating and cooling procedures were repeated to provide statistically significant data for the 78 samples for each ALG concentration. The crystal nucleation induction time for the vials was monitored continuously with an inverted microscope to determine the average induction time of nucleation. The onset of each crystallization event was detected optically; when the first crystal was observed the frame number was recorded. Frames were taken at 5-min intervals. The average nucleation induction time, $\tau$, was determined from a statistical analysis of the induction time data, based on the knowledge that nucleation follows a Poisson distribution[50], $P(t) = e^{(-t/\tau)}$, where $P$ is the probability that no nucleation event occurs within time $t$. The total number of vials as a function of time was also monitored during the experiment.

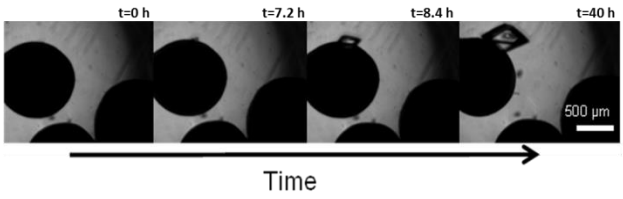


**Figure 4.** Optical micrographs from time-lapsed nucleation induction time experiments. ACM crystals grow in contact with ALG particles from a supersaturated ethanol solution at 10ºC.

Ranking the average induction time values for the different ALG concentrations employed as heteronucleants (Table 1), shows that induction time decreases with increasing ALG concentration. These results can be explained as the interplay of mesh-induced confinement and favorable solute-polymer interactions. A mechanistic explanation can be constructed thinking of these effects separately. Assuming the polymer-solute interaction is not varying for different ALG concentrations, the induction time is expected to increase with increasing ALG concentration due to decreasing mesh size (Figure 2d). The hydrogel mesh can be thought of as a container (of volume $\xi^3$) holding a constant concentration. With decreasing mesh size i.e. nucleation volume, the number of molecules attempting to form critical nuclei decreases and, hence induction time increases. However thinking about only polymer-solute interaction assuming mesh size is constant produces an opposite effect. Solute-polymer interactions are expected to get stronger with increasing ALG concentration. In other words, the number of polymer chains that solute API encounters per volume increases (with increasing ALG concentration) leading to faster nucleation kinetics and, hence smaller induction times[18, 20, 26]. Putting mechanistic explanations of the two effects together, we can explain the observed trend. As the ALG concentration increases, the inhibiting volume effect of mesh size is counteracted by

increasing solute-polymer interactions leading to faster nucleation kinetics. These observations are in accordance with previously published results[20, 26].

Furthermore, at low ALG concentrations (<6%), the presence of ALG particles tends to inhibit nucleation kinetics with respect to bulk (control in Table 1) whereas at high ALG concentrations (>8%), the presence of ALG hydrogels as heteronucleants tends to promote nucleation of ACM from solution. We explain this behavior with two possible scenarios: (i) the absence of solute-polymer interactions in control, (ii) the gradient of partitioning coefficient with respect to ALG concentration. The control measurements without ALG hydrogels can be thought of as a hypothetical hydrogel with large mesh size absent solute-polymer interactions. The absence of solute-polymer interaction might counteract the nucleation time enhancement due to large mesh size hence leading to intermediate induction times. The other working hypothesis is attributed to the gradient of the partitioning coefficient. At low ALG concentrations (<6%), due to the relatively large partitioning coefficient (κ), the concentration of solute in continuous phase (Figure 3) is lower than in the control and, hence larger induction times than for the bulk are observed. As our induction time measurements are more likely to capture crystals growing on the surface of hydrogel than ones deeply engulfed and possibly trapped in the hydrogel, the concentration in the bulk might directly influence the nucleation kinetics. Such behavior is not observed in previous studies of nucleation kinetics of ACM in the presence of hydrogels where partitioning coefficient is reported to be constant for different mesh sizes used[18-20, 26, 51]. As the characteristic time for ACM to diffuse into hydrogels is in the order of minutes, we are believe ACM in hydrogels is in equilibrium with the ACM in the surroundings (Supporting Information).

**Table 1.** Summary of average induction time (**τ**) measurements for the ALG particles of different concentrations used as heteronucleants during the crystallization of ACM from a supersaturated ethanol solution at 10°C.

| **Sample** | **τ (hrs.)** | **error (hrs.)** | **linearity** |
|---|---|---|---|
| Control | 15.3 | 0.31 | 0.99 |
| 4% ALG | 24.7 | 1.4 | 0.92 |
| 6% ALG | 12.8 | 0.23 | 0.97 |
| 8% ALG | 16.5 | 0.50 | 0.95 |
| 10% ALG | 9.5 | 0.18 | 0.98 |
| 12% ALG | 7.7 | 0.10 | 0.99 |

To determine the potential use of ALG particles to encapsulate industrially relevant amounts of hydrophilic drug materials, the loading capacities of the ALG hydrogels with varying mesh sizes are tested via incubating API with the hydrogels. ACM is used as a model compound for this investigation. In this method, ALG particles are equilibrated in a saturated solution (200mg/mL ACM in ethanol at 27°C). At the end of the equilibration time, solid ACM remaining in the solution indicates that the system has reached equilibrium and no more partitioning into the ALG matrix will occur. The particles are washed with iced water and filtered. Scanning electron microscopy (SEM) is used to corroborate that the drug materials have been deposited inside the particle. A cross section of an ALG particle in which no drug product has been loaded i.e. control

(Figure 3b) and another cross section of an ALG particle in which drug product has been loaded using the solvent exchange method are shown in Figure 3c.

To determine the amount of drug loaded, a known amount of the ALG particles are transferred to a known amount of solvent (water) and stirred at a constant temperature. The dissolution or release of the drug is monitored over time using UV-Vis spectrometry and the concentration of the drug at equilibrium is determined using its absorbance. It is observed that at lower ALG compositions the amount of drug loaded is more than twice the amount loaded at higher ALG concentrations (Figure 5). This effect might be due to the larger average mesh size of the lower ALG concentrations and also supports the findings with regards to the solute partition coefficient, which decreases with increasing ALG concentration.

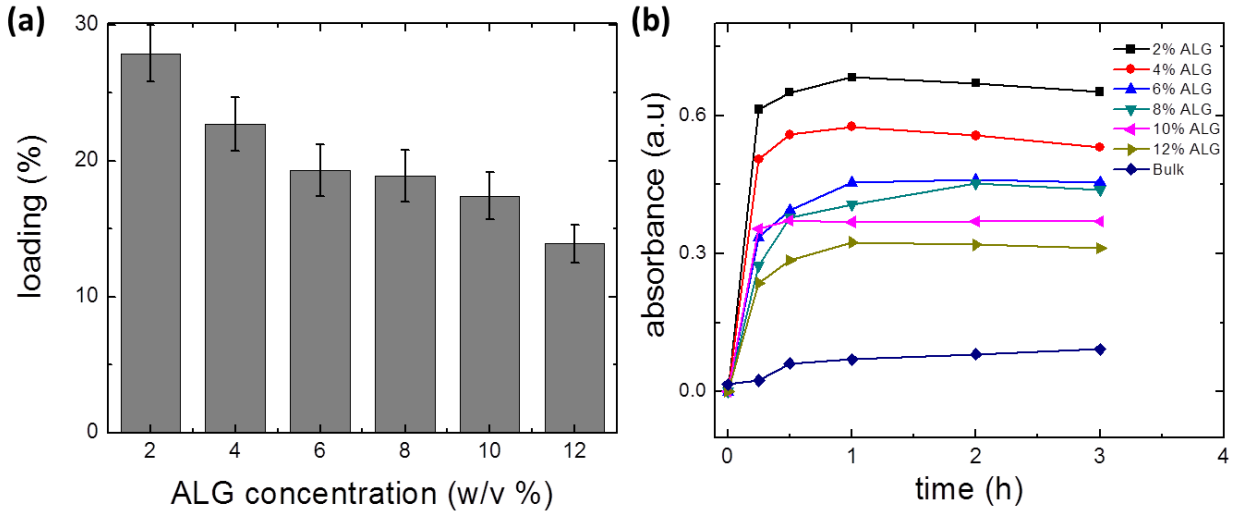


**Figure 5.** (a) ACM loading in hydrated hydrogels calculated by equilibrium partitioning for various ALG concentrations. (b) UV-Vis absorbance measurements for ACM released from the ALG particles as a function of time in water.

Following the equilibrium partitioning procedure, the loaded ALG particles are analyzed to determine the solvent retained -a very important parameter in pharmaceutical formulations. Thermogravimetric analysis (TGA) is used to determine the solvent loss as a function of temperature. It is observed that for lower ALG concentrations the percent weight loss is higher when the ALG beads are heated between 40-200ºC, indicating a higher percentage of solvent (ethanol and water) entrapped inside the pores of these hydrogels. At higher ALG concentrations, the percent weight loss is lower within the same temperature range, indicating that lower amounts of solvents (ethanol and water) remained inside the particles after they are loaded with the drug (Supporting Information). In order to reduce the solvent content without having to vacuum-dry the loaded samples, which would change the porosity and dissolution behavior of the encapsulated drug material, the ALG particles are directly compressed into tablets. About 250 mg of ALG particles are pressed with a 6-mm tablet maker in order to form a tablet (Supporting Information). TGA analysis is performed to determine the solvent content in the tablet. Thermograms showed that in the pressed ALG particles, the percentage weight loss is reduced by about 30% indicating that most of the solvent was removed by direct compression (Supporting Information). Moreover, the 15% weight loss occurring initially in the thermogram of the loaded and compressed ALG particles corresponds to the drug loaded, which is about 17% when determined by equilibrium partitioning.

In order to determine if the drug material encapsulated in the ALG particle is crystalline or amorphous, powder X-ray diffraction (PXRD) analysis is employed. Diffractograms of the various loaded ALG beads of different concentrations suggest that all of the loaded material is crystalline (Figure 6). In general, smaller and lower numbers of diffraction peaks are observed in the high percent ALG particles than in the lower percent ALG particles. This phenomenon might

be due to the smaller size of the pores at higher ALG concentrations, which might lead to the presence of submicron size crystals that would be harder to detect by this technique. Moreover, PXRD indicates that at all ALG concentrations used in the encapsulation studies, the thermodynamically stable form of ACM, form I, is obtained.

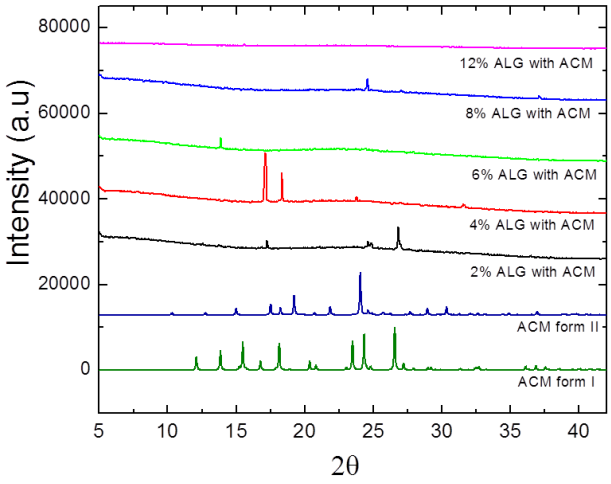


**Figure 6.** Experimental PXRD of loaded ALG particles at different concentrations, indicating that crystals of ACM form I have been encapsulated into the ALG particles.

By carefully selecting the material properties and the production techniques, we investigate the utility of emulsion laden-hydrogels (Figure 7) in carrying and crystallizing the model hydrophobic API, FEN and their potential as biocompatible final dosage formulations. We first investigate which solvents can be used and trapped inside hydrogels. The solvents to be used must satisfy the following criteria: (i) they have to be chosen from pharmaceutically acceptable organic solvents; (ii) they should dissolve large amounts of model hydrophobic APIs; (iii) they should be amenable to emulsification and encapsulation within hydrogels. We identified heptane (HEP) and ethyl acetate (EA) as potential candidates due to their pharmaceutically acceptable nature. We studied their emulsification with different methods and their ability to act as

hydrophobic API carrying liquid pockets within hydrogels. As emulsions trapped in hydrogel matrix provide a more favorable environment for FEN to partition compared to the surrounding aqueous environment, we expect strong partitioning of FEN within emulsion droplets only a small fraction of FEN can escape to aqueous environment (Supporting Information for a more detailed discussion).

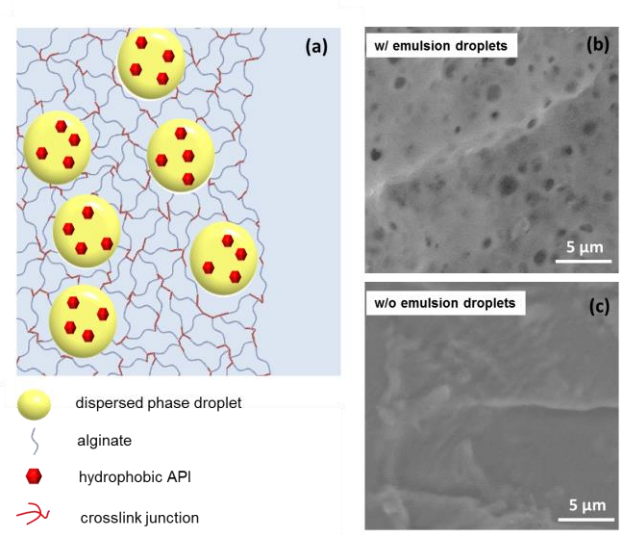


**Figure 7.** (a) Illustration showing emulsion laden hydrogels loaded with hydrophobic API, fenofibrate (FEN). (b) Cross section of environmental scanning electron microscopy (ESEM) image of ALG hydrogels with emulsion droplets and (c) without emulsion droplets serving as control for panel (b). The continuous phase contains 2% ALG and the volume fraction of the dispersed phase is 30% (v/v) FEN in heptane.

First, we investigate which emulsification method is suitable for our purpose on the basis of loading. The emulsion-laden hydrogels with heptane as the dispersed phase are synthesized as described before with different emulsion volume fractions ranging between 10 to 50% using two different emulsification techniques: magnetic stirring and high pressure homogenization (HPH)

(Figure 8a). Prior to crosslinking, we determine the droplet size in emulsions prepared with both techniques. The sizes of droplets emulsified by magnetic stirring are around 130 μm in diameter with COV of 60% whereas emulsion droplets prepared by HPH are approximately 0.72 μm in diameter with COV of 22%. The loading of FEN increases with increasing volume fraction as expected in samples prepared with both emulsification techniques (Figure 8a). However, the error bars in measured loading are significantly smaller with HPH compared to magnetic stirring. Large variations in API loading are undesired in the pharmaceutical industry as they directly affect the dosage consistency and reproducibility. We hypothesize that the large variation in loading might be due to the relatively large mean droplet diameter and the polydispersity characteristic of magnetic stirring. Magnetic stirring is a cheap yet crude emulsification technique that results in relatively large droplets with large size distributions. These large variations in loading can be understood in terms of terminal velocity ($V_t$). The terminal velocity a drop of diameter (d) and density of $\rho_d$ creaming in surrounding medium of density $\rho_c$ and viscosity μ is given by $V_t \sim \frac{d^2(\rho_d - \rho_c)}{\mu}$ using the creeping flow assumption. The larger droplets cream faster in the finite time required for transferring the emulsified sample after its homogenization to the dripping processes described in Methods and Materials section. The creaming of emulsions droplets in precrosslinked solution generates gradients in amounts of encapsulated emulsions and, hence loading among crosslinked ALG beads. The emulsions prepared by HPH are called nanoemulsions and they have both smaller droplet diameter and polydispersity [38, 52]. As evident from ESEM images given in Figure 7b, the size of nanoemulsion droplets did not change after crosslinking. Furthermore, nanoemulsions are commonly used in the cosmetics, food and pharmaceutical industry due to their long-term stability. Hence we identify HPH as an optimum emulsification method for our purpose.

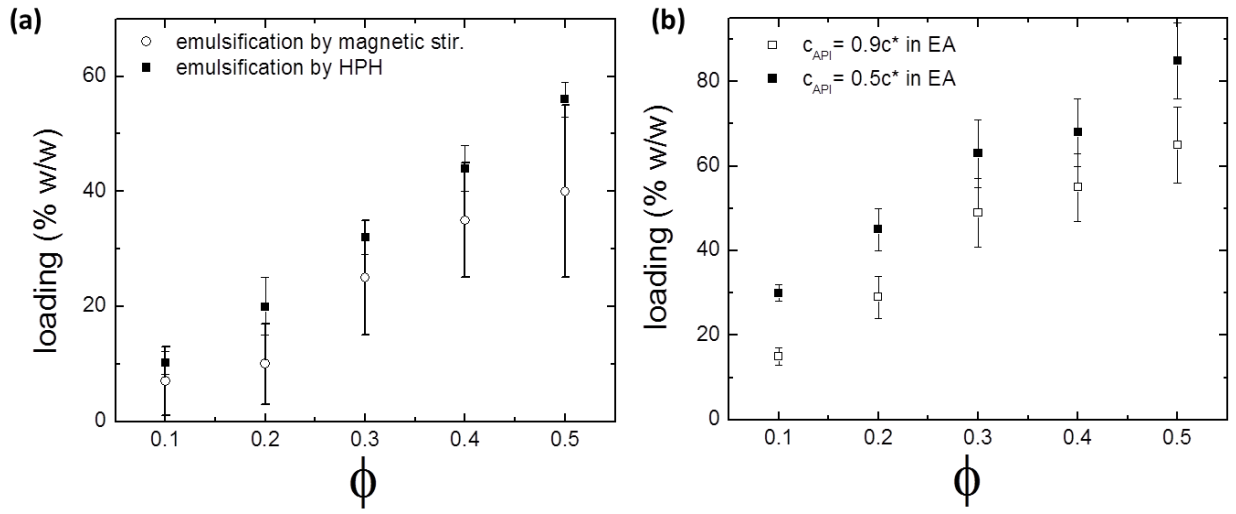


**Figure 8**. (a) Loading (% weight by weight) of FEN in emulsion-laden hydrogels prepared by different emulsification techniques. (b) Loading (% weight by weight) of FEN in ethyl acetate with two FEN concentrations for varying emulsion volume fractions measured by evaporation method.

Secondly, we investigate which solvent is more suitable for preparing emulsion-laden hydrogels and how we can optimize loading --a critical parameter in industrial practice. The loading is a function of the ALG concentration in the continuous phase ($C_{ALG}$), the concentration of API dissolved in the dispersed phase ($C_{API}$), and the volume fraction of the dispersed phase in continuous phase (φ). A rational optimization is required for designing emulsion-laden hydrogels to achieve maximum loading. The maximum φ that can be used is dictated by how densely emulsions can be packed [38]. The maximum $C_{API}$ is dictated by the solubility of FEN in dispersed organic phase. The solubility of FEN in heptane is slightly above 9 mg/mL at 25 °C. The solubility (c*) of FEN in EA is significantly larger, 600 mg/mL. Furthermore, EA has low vapor pressure at room temperature, which makes it an ideal candidate for effectively removing

residual solvent. As expected we managed to load larger amounts of FEN with EA compared to HEP (Figure 8 a b). However, we observed undesired precipitation of FEN in precrosslinked emulsion. We believe this precipitation is due to moderate solubility of EA in water. We counteracted this by reducing the concentration of FEN below its saturation value ($c_{API}$=0.5c* and 0.9c*). By reducing the concentration of FEN in emulsion droplets, we effectively decrease the amount of FEN precipitating and, thus reached relatively high loading values (~80%).

Furthermore, other process and product parameters need to be taken into account while designing API-carrying emulsion-laden hydrogels. For instance, at high volume fractions ($\varphi$ > 50%), crosslinking of emulsion by the dripping method becomes extremely difficult due to the high viscosity and the jamming of emulsions in the dripping needle. Another critical product parameter is the mechanical integrity of hydrogel beads, which is influenced by $C_{ALG}$ and $\varphi$. At low $C_{ALG}$ and high $\varphi$, the hydrogel easily breaks and disintegrates.

Through systematic investigation of solvent types and emulsification methods, we designed an emulsion-laden hydrogel formulation that can carry industrially relevant amounts of a model hydrophobic API. The next step is to check if the emulsion-laden hydrogels can crystallize FEN. In order to identify whether the FEN encapsulated inside the ALG matrix is crystalline or amorphous, three characterization techniques are employed: optical microscopy, PXRD and differential scanning calorimetry (DSC). For optical microscopy, we prepared emulsion-laden hydrogel sandwiched between two glass slides (Supporting Information for detailed procedure). We have chosen to prepare emulsions with magnetic stirring so that the large size of droplets will enable light microscopy. The sample is cooled it down to 10°C on a microscope stage and imaged using time-lapse microscopy. After four hours, we observed FEN crystals particularly in large droplets as shown in Figure 9a whereas the control with emulsion droplets containing no

API did not show crystallization. This observation proves that FEN can be crystallized inside emulsion-laden hydrogels. The experimental diffractogram of FEN carrying emulsion-laden ALG particles prepared by HPH indicate that crystals of FEN have formed inside the ALG hydrogels (Figure 9b). The intensity of the diffraction in the peaks present is not high enough to determine the percent of crystallinity and, therefore further analysis with DSC is required. Thermographs are obtained using empty ALG beads, an FEN standard, and ALG beads loaded with FEN at different volume fractions with different solvents (HEP&EA) in Figure 9c. From these thermographs it can be concluded that FEN loaded into both HEP and EA during this investigation, produces crystalline FEN. Crystalline FEN standards and FEN-loaded emulsion laden hydrogels all produce peaks at 78 °C demonstrating the existence of crystalline FEN within. We also looked at the dissolution behavior of dried emulsion-laden hydrogels; we observed that 80% of the FEN dissolved within four hours followed by a slower release rate. This is two-stage release profile is observed in other polymeric delivery mechanisms as well.

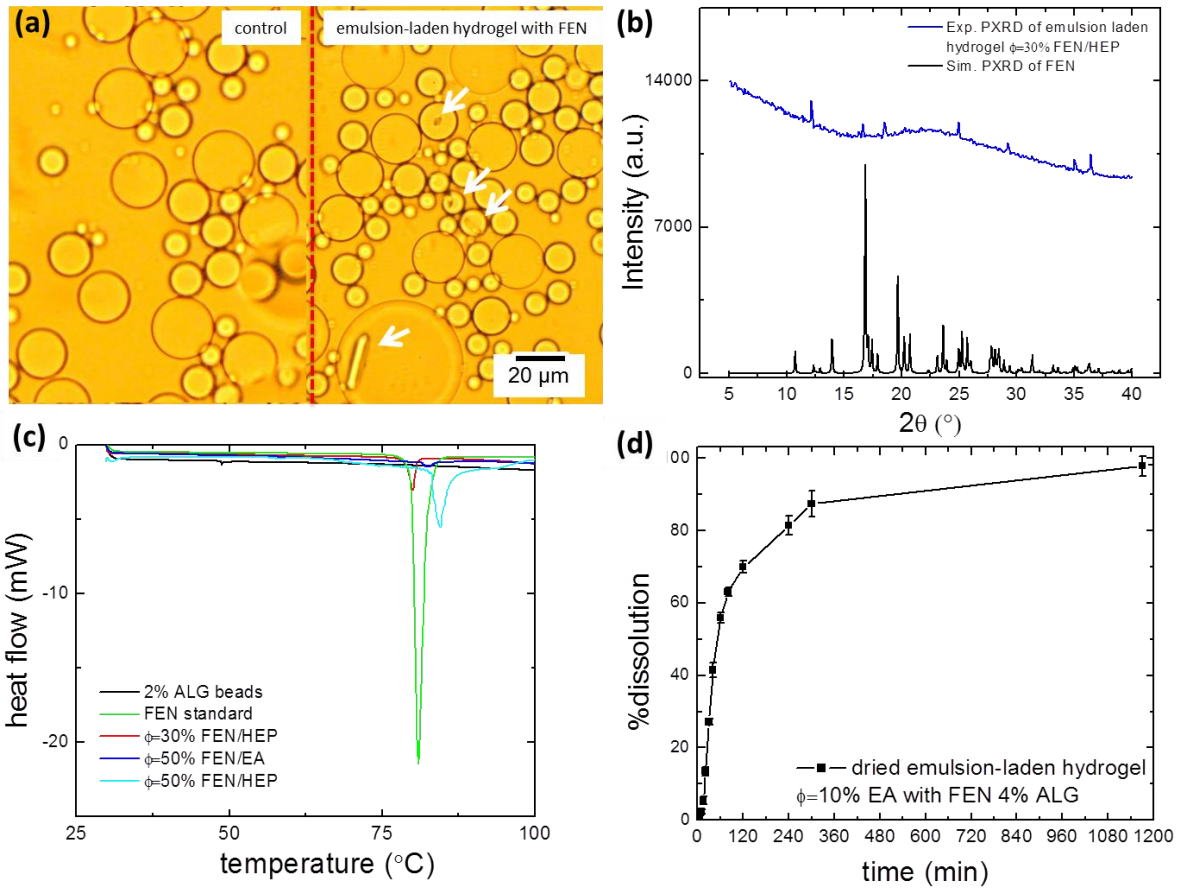


**Figure 9.** Confirmation of FEN crystallization inside emulsion-laden hydrogels. Panel (a) the control: emulsion droplets encapsulated in 2% ALG matrix prepared by magnetic stirring without FEN and with FEN. FEN crystals growing inside emulsion droplets carrying FEN is observed. Both samples have been cooled to 10°C and time lapse images are taken. Panel (a) shows images taken at t=4 hrs. Details on sample preparation appear in the Supporting Information. Panel (b) shows PXRD data of API loaded emulsion laden hydrogels prepared by HPH emulsification. Panel (c) shows the DSC data for FEN loaded hydrogels with both HEP and EA. Panel (d) shows the dissolution profile of dried emulsion laden hydrogels.

In this study we investigated the utility of ALG hydrogels as a versatile biocompatible vehicle for crystallizing and encapsulating APIs that exhibit dramatically different solubilities in

water due to their distinct chemical structures. For hydrophilic model API (ACM), we investigated the potential of ALG hydrogels as heteronucleants to influence nucleation induction times from solution and their ability to encapsulate ACM. Our results indicate that a cut-off in ALG concentration (hence hydrogel mesh size) exists in which ALG particles of different concentrations are able to promote the nucleation of ACM from solution. Below this cut-off, ALG particles suppress the nucleation. We attribute these results to the interplay between the mesh-size-induced confinement and the solute-polymer interactions. Furthermore, the amount of ACM that can be loaded into hydrogels through thermodynamic partitioning depends on mesh size. Hence a trade-off is required to design ALG hydrogels capable of functioning as heteronucleants in a crystallization process while carrying large amounts of the model hydrophilic API. For the hydrophobic API, FEN, we demonstrated efficient loading (~up to 82% w/w) and crystallization of FEN in emulsion-laden hydrogels. We identified the optimum emulsification method, solvent type, volume fraction of dispersed phase and concentration of API within the dispersed phase to maximize loading. Our results suggest that emulsion-laden ALG hydrogels prepared with high pressure homogenization utilizing ethyl acetate as the dispersed phase might offer fine control over dosage and dosage consistency while achieving significant loading of FEN. The methodologies presented open new investigation alleys for designing biocompatible materials that can act as heteronucleants while encapsulating large amounts of drugs with vastly different water solubilities. Furthermore, ALG hydrogels and emulsion-laden hydrogels can be used as final drug formulation in a continuous manufacturing scheme due to their biocompatible nature and their ability to carry APIs with diverse chemical nature.

ASSOCIATED CONTENT

**Supporting Information**. Detailed experimental procedures, rheological determination of ALG mesh size, thermogravimetric analysis (TGA), induction time analysis and tablet preparation. This material is available free of charge via the Internet at http://pubs.acs.org.

AUTHOR INFORMATION

Corresponding authors pdoyle@mit.edu ,

**Author Contributions**

The manuscript was written through contributions of all authors. All authors have given approval to the final version of the manuscript. ‡These authors contributed equally.

ACKNOWLEDGMENT

We acknowledge the Novartis-MIT Continuous Manufacturing Center for financial support. HBE acknowledges R.Shaw from MIT UROP program, A. Ryan from MIT machine shop for their support in experiments.

REFERENCES

(1) Debenedetti, P. G., *Metastable liquids: concepts and princibles*. ed.; Princeton University Press: Princeton,NJ, 1996.
(2) Mullin, J. W., *Crystalization*. 4 ed.; Butterworth-Heinemann:Oxford: Boston, 2001.
(3) Oxtoby, D. W., Nucleation of first-order phase transitions. *Accounts Chem Res* **1998,** 31, (2), 91-97.
(4) Price, C. P.; Grzesiak, A. L.; Matzger, A. J., Crystalline polymorph selection and discovery with polymer heteronuclei. *J Am Chem Soc* **2005,** 127, (15), 5512-5517.
(5) Berman, A.; Ahn, D. J.; Lio, A.; Salmeron, M.; Reichert, A.; Charych, D., Total Alignment of Calcite at Acidic Polydiacetylene Films - Cooperativity at the Organic-Inorganic Interface. *Science* **1995,** 269, (5223), 515-518.
(6) Aizenberg, J.; Black, A. J.; Whitesides, G. H., Oriented growth of calcite controlled by self-assembled monolayers of functionalized alkanethiols supported on gold and silver. *J Am Chem Soc* **1999,** 121, (18), 4500-4509.

(7) Aizenberg, J.; Black, A. J.; Whitesides, G. M., Control of crystal nucleation by patterned self-assembled monolayers. *Nature* **1999,** 398, (6727), 495-498.
(8) Bunker, B. C.; Rieke, P. C.; Tarasevich, B. J.; Campbell, A. A.; Fryxell, G. E.; Graff, G. L.; Song, L.; Liu, J.; Virden, J. W.; Mcvay, G. L., Ceramic Thin-Film Formation on Functionalized Interfaces through Biomimetic Processing. *Science* **1994,** 264, (5155), 48-55.
(9) Lee, A. Y.; Lee, I. S.; Dettet, S. S.; Boerner, J.; Myerson, A. S., Crystallization on confined engineered surfaces: A method to control crystal size and generate different polymorphs. *J Am Chem Soc* **2005,** 127, (43), 14982-14983.
(10) Carter, P. W.; Ward, M. D., Topographically Directed Nucleation of Organic-Crystals on Molecular Single-Crystal Substrates. *J Am Chem Soc* **1993,** 115, (24), 11521-11535.
(11) Gavish, M.; Wang, J. L.; Eisenstein, M.; Lahav, M.; Leiserowitz, L., The Role of Crystal Polarity in Alpha-Amino-Acid Crystals for Induced Nucleation of Ice. *Science* **1992,** 256, (5058), 815-818.
(12) Hiremath, R.; Basile, J. A.; Varney, S. W.; Swift, J. A., Controlling molecular crystal polymorphism with self-assembled monolayer templates. *J Am Chem Soc* **2005,** 127, (51), 18321-18327.
(13) Page, A. J.; Sear, R. P., Heterogeneous nucleation in and out of pores. *Phys Rev Lett* **2006,** 97, (6).
(14) Page, A. J.; Sear, R. P., Crystallization Controlled by the Geometry of a Surface. *J Am Chem Soc* **2009,** 131, (48), 17550-17551.
(15) Ha, J. M.; Wolf, J. H.; Hillmyer, M. A.; Ward, M. D., Polymorph selectivity under nanoscopic confinement. *J Am Chem Soc* **2004,** 126, (11), 3382-3383.
(16) Beiner, M.; Rengarajan, G. T.; Pankaj, S.; Enke, D.; Steinhart, M., Manipulating the crystalline state of pharmaceuticals by nanoconfinement. *Nano Lett* **2007,** 7, (5), 1381-1385.
(17) Rengarajan, G. T.; Enke, D.; Steinhart, M.; Beiner, M., Stabilization of the amorphous state of pharmaceuticals in nanopores. *J Mater Chem* **2008,** 18, (22), 2537-2539.
(18) Diao, Y.; Whaley, K. E.; Helgeson, M. E.; Woldeyes, M. A.; Doyle, P. S.; Myerson, A. S.; Hatton, T. A.; Trout, B. L., Gel-Induced Selective Crystallization of Polymorphs. *J Am Chem Soc* **2012,** 134, (1), 673-684.
(19) Diao, Y.; Helgeson, M.; Doyle, P.; Myerson, A.; Hatton, T. A.; Trout, B., Design of polymeric substrates for controlled molecular crystallization. *Abstr Pap Am Chem S* **2011,** 242.
(20) Diao, Y.; Helgeson, M. E.; Siam, Z. A.; Doyle, P. S.; Myerson, A. S.; Hatton, T. A.; Trout, B. L., Nucleation under Soft Confinement: Role of Polymer-Solute Interactions. *Cryst Growth Des* **2012,** 12, (1), 508-517.
(21) Eral, H. B.; Mugele, F.; Duits, M. H. G., Colloidal Dynamics Near a Particle-Covered Surface. *Langmuir* **2011,** 27, (20), 12297-12303.
(22) Eral, H. B.; Oh, J. M.; van den Ende, D.; Mugele, F.; Duits, M. H. G., Anisotropic and Hindered Diffusion of Colloidal Particles in a Closed Cylinder. *Langmuir* **2010,** 26, (22), 16722-16729.
(23) Williams, I.; Oguz, E. C.; Bartlett, P.; Lowen, H.; Royall, C. P., Direct measurement of osmotic pressure via adaptive confinement of quasi hard disc colloids. *Nature Communications* **2013,** 4.
(24) Oguz, E. C.; Marechal, M.; Ramiro-Manzano, F.; Rodriguez, I.; Messina, R.; Meseguer, F. J.; Lowen, H., Packing Confined Hard Spheres Denser with Adaptive Prism Phases. *Phys Rev Lett* **2012,** 109, (21).

(25) Suleimanov, Y. V., Surface Diffusion of Hydrogen on Ni(100) from Ring Polymer Molecular Dynamics. *J Phys Chem C* **2012,** 116, (20), 11141-11153.
(26) Diao, Y.; Helgeson, M. E.; Myerson, A. S.; Hatton, T. A.; Doyle, P. S.; Trout, B. L., Controlled Nucleation from Solution Using Polymer Microgels. *J Am Chem Soc* **2011,** 133, (11), 3756-3759.
(27) Jackson, C. L.; McKenna, G. B., Vitrification and crystallization of organic liquids confined to nanoscale pores. *Chem Mater* **1996,** 8, (8), 2128-2137.
(28) Augst, A. D.; Kong, H. J.; Mooney, D. J., Alginate hydrogels as biomaterials. *Macromol Biosci* **2006,** 6, (8), 623-633.
(29) Martinsen, A.; Skjakbraek, G.; Smidsrod, O., Alginate as Immobilization Material .1. Correlation between Chemical and Physical-Properties of Alginate Gel Beads. *Biotechnol Bioeng* **1989,** 33, (1), 79-89.
(30) Moe, S. T.; Elgsaeter, A.; Skjakbraek, G.; Smidsrod, O., A New Approach for Estimating the Cross-Link Density of Covalently Cross-Linked Ionic Polysaccharide Gels. *Carbohyd Polym* **1993,** 20, (4), 263-268.
(31) Moe, S. T.; Skjak-Braek, G.; Smidsrod, O., Covalently cross-linked sodium alginate beads. *Food Hydrocolloid* **1991,** 5, (1-2), 119-123.
(32) Strand, B. L.; Morch, Y. A.; Skjak-Braek, G., Alginate as immobilization matrix for cells. *Minerva Biotecnol* **2000,** 12, (4), 223-233.
(33) Takka, S.; Acarturk, F., Calcium alginate microparticles for oral administration: I: effect of sodium alginate type on drug release and drug entrapment efficiency. *J Microencapsul* **1999,** 16, (3), 275-290.
(34) Lipinski, C. A.; Lombardo, F.; Dominy, B. W.; Feeney, P. J., Experimental and computational approaches to estimate solubility and permeability in drug discovery and development settings. *Adv Drug Deliver Rev* **2012,** 64, 4-17.
(35) Inoue, T.; Chen, G. H.; Hoffman, A. S.; Nakamae, K., A hydrophobically modified bioadhesive polymeric carrier for controlled drug delivery to mucosal surfaces. *J Bioact Compat Pol* **1998,** 13, (1), 50-64.
(36) Gou, M. L.; Li, X. Y.; Dai, M.; Gong, C. Y.; Wang, X. H.; Xie, Y.; Deng, H. X.; Chen, L. J.; Zhao, X.; Qian, Z. Y.; Wei, Y. Q., A novel injectable local hydrophobic drug delivery system: Biodegradable nanoparticles in thermo-sensitive hydrogel. *Int J Pharmaceut* **2008,** 359, (1-2), 228-233.
(37) Jeong, B.; Bae, Y. H.; Kim, S. W., Drug release from biodegradable injectable thermosensitive hydrogel of PEG-PLGA-PEG triblock copolymers. *J Control Release* **2000,** 63, (1-2), 155-163.
(38) Mason, T. G.; Wilking, J. N.; Meleson, K.; Chang, C. B.; Graves, S. M., Nanoemulsions: formation, structure, and physical properties. *J Phys-Condens Mat* **2006,** 18, (41), R635-R666.
(39) McClements, D. J., Crystals and crystallization in oil-in-water emulsions: Implications for emulsion-based delivery systems. *Adv Colloid Interfac* **2012,** 174, 1-30.
(40) McClements, D. J., Nanoemulsions versus microemulsions: terminology, differences, and similarities. *Soft Matter* **2012,** 8, (6), 1719-1729.
(41) An, H. Z.; Helgeson, M. E.; Doyle, P. S., Nanoemulsion Composite Microgels for Orthogonal Encapsulation and Release. *Adv Mater* **2012,** 24, (28), 3838-3844.
(42) Jagadeesan, D.; Nasimova, I.; Gourevich, I.; Starodubtsev, S.; Kumacheva, E., Microgels for the Encapsulap:\tion and Stimulus-Responsive Release of Molecules with Distinct Polarities. *Macromol Biosci* **2011,** 11, (7), 889-896.

(43) Josef, E.; Zilberman, M.; Bianco-Peled, H., Composite alginate hydrogels: An innovative approach for the controlled release of hydrophobic drugs. *Acta Biomater* **2010,** 6, (12), 4642-4649.
(44) Turco, G.; Donati, I.; Grassi, M.; Marchioli, G.; Lapasin, R.; Paoletti, S., Mechanical Spectroscopy and Relaxometry on Alginate Hydrogels: A Comparative Analysis for Structural Characterization and Network Mesh Size Determination. *Biomacromolecules* **2011,** 12, (4), 1272-1282.
(45) Larson, R., *The Structure and Rheology of Complex Fluids*. ed.; Oxford University Press: New York 1999.
(46) Gardel, M. L.; Shin, J. H.; MacKintosh, F. C.; Mahadevan, L.; Matsudaira, P.; Weitz, D. A., Elastic Behavior of cross-linked and bundled actin networks. *Science* **2004,** 304, (5675), 1301-1305.
(47) Flory, P. J., *Principles of Polymer Chemistry*. ed.; Oxford University

Press: Ithaca,NY, 1953.
(48) Chan, A. W.; Whitney, R. A.; Neufeld, R. J., Kinetic controlled synthesis of pH-responsive network alginate. *Biomacromolecules* **2008,** 9, (9), 2536-2545.
(49) Jamzad, S.; Fassihi, R., Role of surfactant and pH on dissolution properties of fenofibrate and glipizide - A technical note. *Aaps Pharmscitech* **2006,** 7, (2).
(50) Diao, Y.; Harada, T.; Myerson, A. S.; Hatton, T. A.; Trout, B. L., The role of nanopore shape in surface-induced crystallization. *Nat Mater* **2011,** 10, (11), 867-871.
(51) Diao, Y.; Helgeson, M.; Myerson, A.; Hatton, T. A.; Doyle, P.; Trout, B., Rational design of polymeric nucleants for controlling nucleation. *Abstr Pap Am Chem S* **2011,** 241.
(52) Fryd, M. M.; Mason, T. G., Advanced Nanoemulsions. *Annu Rev Phys Chem* **2012,** 63, 493-518.

# Biocompatible Alginate Microgel Particles as Heteronucleants and Encapsulating Vehicles for Hydrophilic and Hydrophobic Drugs

*Huseyin Burak Eral[ǂ], Vilmalí López-Mejías[ǂ], M.O'Mahonny, Bernhardt L. Trout, Allan S. Myerson and Patrick S. Doyle**

Novartis-MIT Center for Continuous Manufacturing and the Department of Chemical Engineering, Massachusetts Institute of Technology, 77 Massachusetts Avenue, E19-502b, Cambridge, MA 02139.

Supporting Information

**Table of content.**

I. Experimental

II. Rheological Characterization

III. Themogravimetric Analysis (TGA)

IV. Nucleation Induction Time Experiments

V. Direct compression into tablets

VI. Efficiency of FEN encapsulation

VII. References

## I. Experimental details.

*Preparation of emulsion laden hydrogels sandwiched between two glass slides*. For confirmation of crystallization inside hydrogels, we have prepared emulsion laden hydrogels sandwiched between two glass slides. First, the emulsion with dispersed phase HEP containing FEN and the continuous phase containing 2% w/v Na-ALG is allowed to be sucked into the sample chamber with capillary forces. After the uncrosslinked emulsion is placed inside the sample holder, the Na-ALG in the continuous phase is cross-linked by immersing the sample chamber into 6% $CaCl_2$ overnight. The sample chamber is prepared by using approximately 100 micron thick polymer film spacer to align two glass slides parallel. The polymer spacer is glued onto the glass slides by heating at 65°C over 30 min. In order to visualize the crystals under microscopy, we prepared relatively large and polydisperse droplets with magnetic stirring.

## II. Rheological characterization:

Rheological characterization was carried out on a TA Instruments AR-G2 stress-controlled rheometer with a 60 mm, 2° upper-cone geometry and temperature-controlled Peltier lower-plate geometry. A solvent trap wetted with deionized water was used to limit sample evaporation. We start with characterizing the rheological behavior of Na-ALG for different ALG concentrations prior to crosslinking. The samples are homogenized prior to measurements with gentle shear at 1 $s^{-1}$. The flow curves at 1% strain are measured by increasing the shear rate from 10 to 1000 $s^{-1}$. At low ALG concentrations (<2%), viscosity is independent of shear rate whereas at higher ALG concentrations solutions showed shear thinning behavior (Figure S1). This is important to realize as dependence of viscosity to shear rate is critical in understanding the process ability of complex fluids. We also conducted small-amplitude oscillatory shear, frequency sweeps are carried out over a range of 1-200 rad $s^{-1}$ at strain amplitude of 0.05%. All the Na-ALG solutions show Newtonian behavior in small amplitude regime as expected.

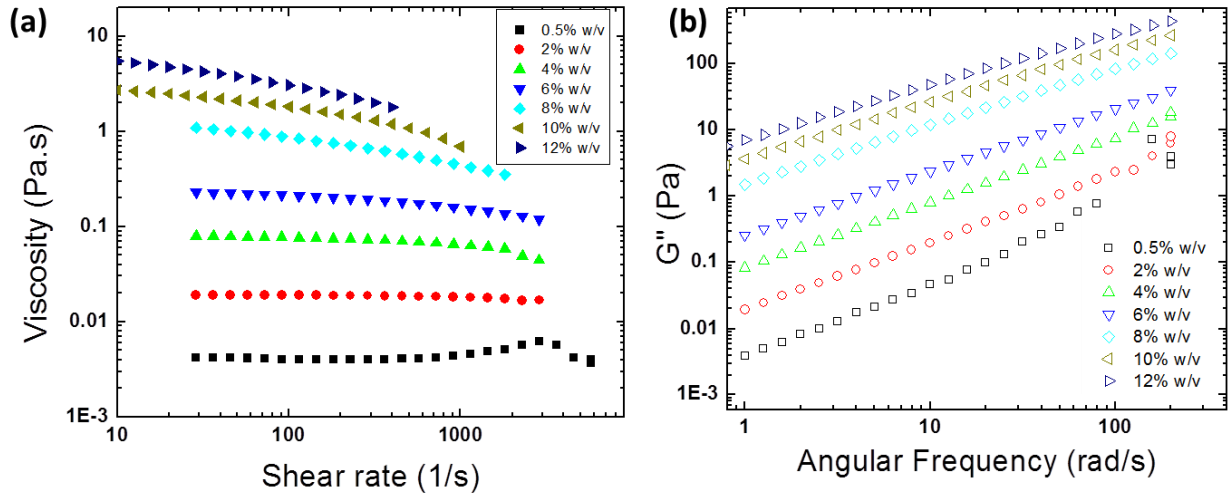


**Figure S1**. (a) Flow curves for different ALG concentrations. (b) Small amplitude oscillatory shear frequency.

***Determination of mesh size from small amplitude rheology measurements.***

The characterization of mesh size for different alginate concentrations is performed by rheology. Disk shaped alginate gels at different polysaccharide concentration, namely, 1, 2, 4, 8, 10 and 12% (w/v), have been prepared in calcium-saturated conditions and their rheological response are recorded (Figure 2c of Main text). In all alginate concentrations considered, the storage (G`) modulus is monotonous and higher than the loss modulus (G``). This describes the hydrogels as strong gels. The frequency sweep test are interpreted in terms of the generalized Maxwell model composed of a sequence of elements in parallel (spring and dashpot) to which an additional spring has been added (Figure 2 of main text). Analogous to a mechanical model shown in inset of Figure 2b of main text, the storage and loss moduli can be modeled as a function frequency ω according to the following equations (S1, S2) also given in Figure 2.

$$G' = Ge + \sum_{i=1}^{n} Gi \frac{(\lambda_i \omega)^2}{1+(\lambda_i \omega)^2} \quad (eq.S1)$$

$$G'' = \sum_{i=1}^{n} Gi \frac{(\lambda_i \omega)^2}{1+(\lambda_i \omega)^2} \quad G_i = \frac{\eta_i}{\lambda_i} \; (eq. S2)$$

where n is the number of Maxwell elements considered $G_i$, $\eta_i$ and $\lambda_i$ represent the spring constant, the dashpot viscosity, and the relaxation time of the $i^{th}$ Maxwell element, respectively. $G_e$ is the spring constant of the last Maxwell element which is purely elastic.

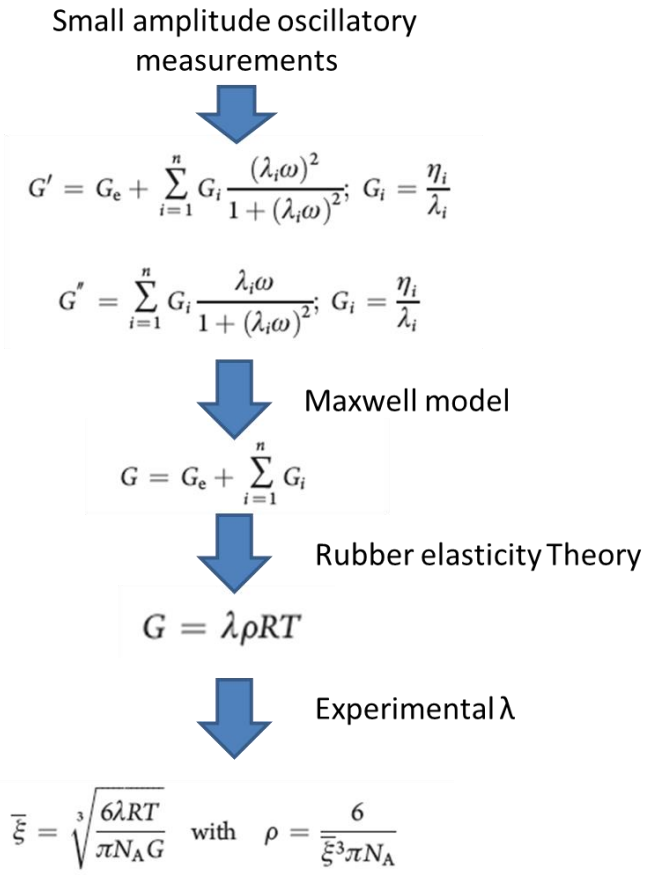


**Figure S2.** Flow diagram for calculations leading to determination of mesh size from oscillatory rheology measurements.

The fitting of the experimental data is performed as described in Figure S2 following the approach of Turco et al[1]. This approach assumes that the relaxation times are not independent each other but they are scaled by a factor 10. The number of the Maxwell elements is selected, based on a statistical procedure, to minimize the product $\chi 2 * N_p$. For our measurements, 4 Maxwell elements are sufficient to describe the

system with 0.99 accuracy. The use of the generalized Maxwell model to describe the alginate system allows determining the shear modulus, G as $G = G_e + \sum_{i=1}^{n} G_i$

*Connecting shear modulus to rubber like elasticity.*

This shear "complex" modulus is found to scale with the total alginate concentration initially an linear manner later slowly saturating. This is in very good agreement with previous findings by Turco and coworkers[2] along with calcium saturated conditions at lower alginate concentrations also Mooney and co-workers[3] in calcium-limited conditions. The shear modulus of the alginate cylinders is interpreted in terms of the rubber elasticity theory, originally developed by Flory[4].

Yet it is important to emphasize that there are fundamental differences between biopolymer gels and elastic rubbers in terms of macromolecular characteristics, such as flexibility. However, recent results have shown that very stiff biopolymers might give rise to networks which are suitably described by a purely entropic approach[5]. This holds when small deformations are considered, that is, under linear stress-strain relationship (linear viscoelastic region). Indeed, a purely entropic approach has also been recently used to calculate the mesh size for alginate hydrogels[2].

As the mechanical characterization performed in the present paper is in the linear viscoelastic region, the entropic contribution can be used in the description of the alginate network. In view of these considerations, the number (per unit volume) of elastically active chains, can be calculated, according to the rubber elasticity theory[4], simply using $G = \alpha \rho RT$ where R is the universal gas constant and T is the absolute temperature. Biopolymer hydrogels display junction zones rather than the cross-linking points described in the original version of the rubber elasticity theory. To take this into account, a front factor,α, is included which, in the case of ideal rubbers, equals 1. Once the α is determined the mesh size ξ, can be calculated from equation S3[4].

$$\xi = \sqrt[3]{\frac{6\alpha RT}{\pi N_A G}} \quad \text{and} \quad \rho = \frac{6}{\xi^3 \pi N_A} \quad (eq.S3)$$

*Discussion about front factor (α).*

In these calculations the front factor needs to be determined accurately to estimate the mesh size. This has been achieved by adapting α values from previous work[2, 3] where the mesh size calculated from rheological data and cryo-TEM has been matched in an effort to calculate the α values for 2% ALG hydrogels prepared under $Ca^{+2}$ saturated conditions. We assume that the front factor should not vary with increasing ALG concentration. We believe this assumption is reasonable as the front factor accounts for deviations from point-like cross links and the nature of crosslinks is not changing with increasing alginate concentration.

## III. Thermogravimetric Analysis (TGA):

Thermograms of the samples were recorded in a TA instruments DSC Q50. Data were analyzed with TA Universal Analysis software Version 4.3A. Samples (1.5-5.0 mg weighed to a precision of 0.0001mg) were placed on hermetic aluminum pans crimped using a TA instrument crimper. Thermal behavior of the samples was studied under a nitrogen purge at 5 ºC/min heating rate, starting at equilibrated temperature of 40° and heating to 400 ºC. The instrument was calibrated with an indium standard.

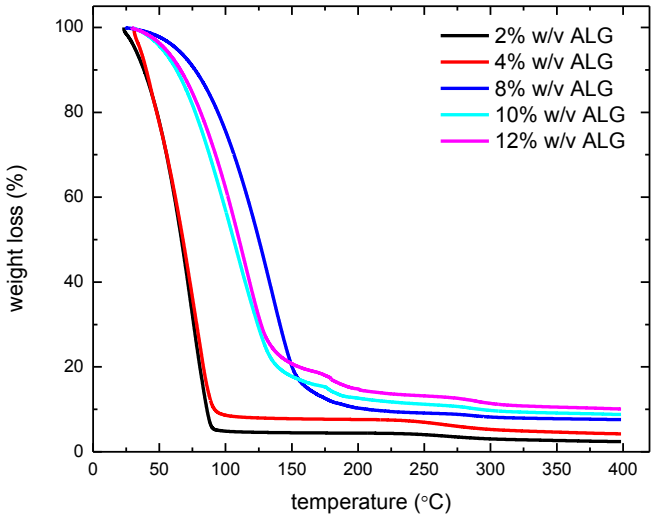

**Figure S3.** Thermographs of as synthesized ALG particles.

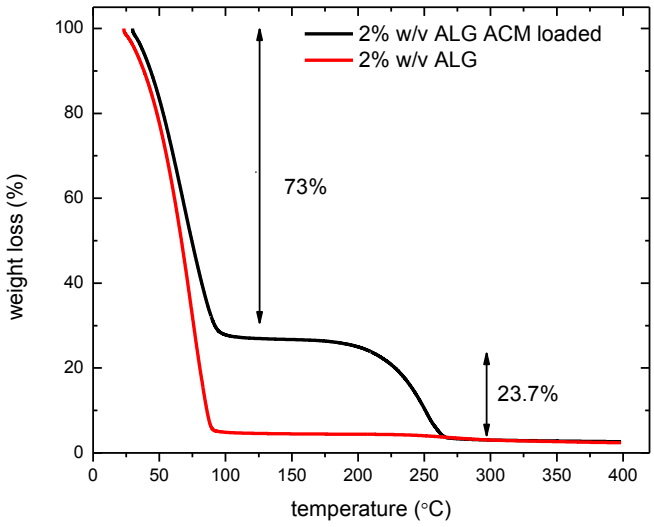


**Figure S4.** Thermographs of (a) 2% ALG particles in red and (b) 2% ALG particles loaded with ACM through solvent exchange method in black.

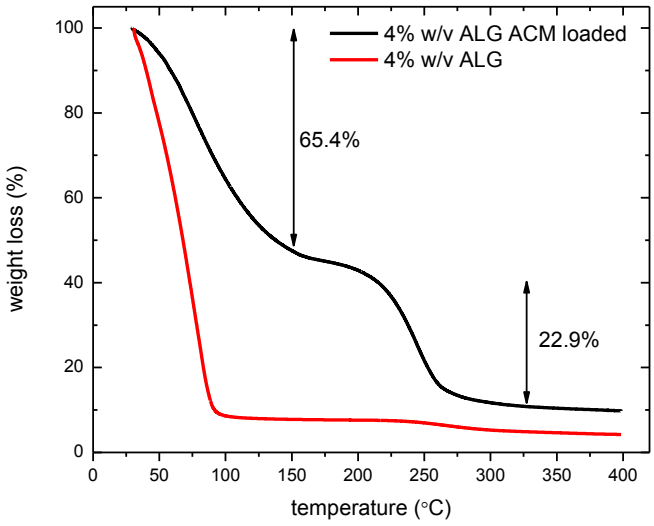

**Figure S5.** Thermographs of (a) 4% ALG particles in red and (b) 4% ALG particles loaded with ACM through solvent exchange method in black.

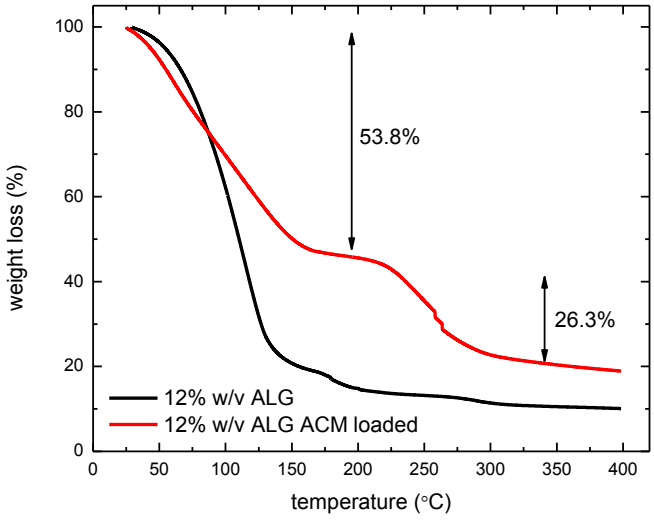


**Figure S6.** Thermographs of (a) 12% ALG particles in red and (b) 12% ALG particles loaded with ACM through solvent exchange method in black.

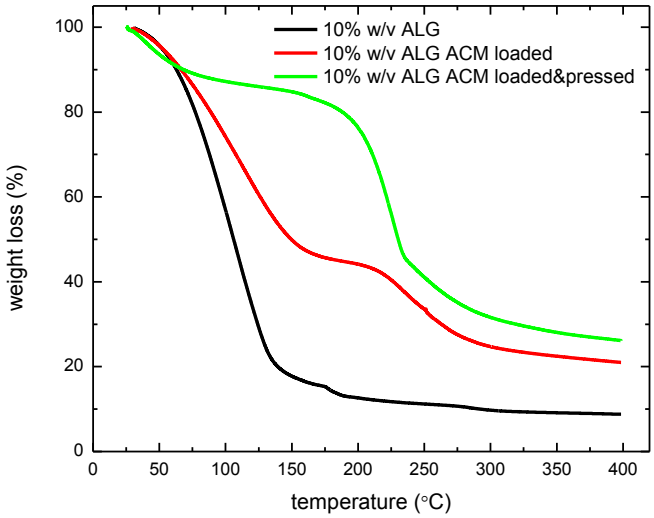

**Figure S7.** Thermographs of (a) 10% ALG particles in black, (b) 10% ALG particles loaded with ACM through solvent exchange method in red, and (c) 10% ALG particles loaded with ACM and then pressed into a table to decrease solvent content.

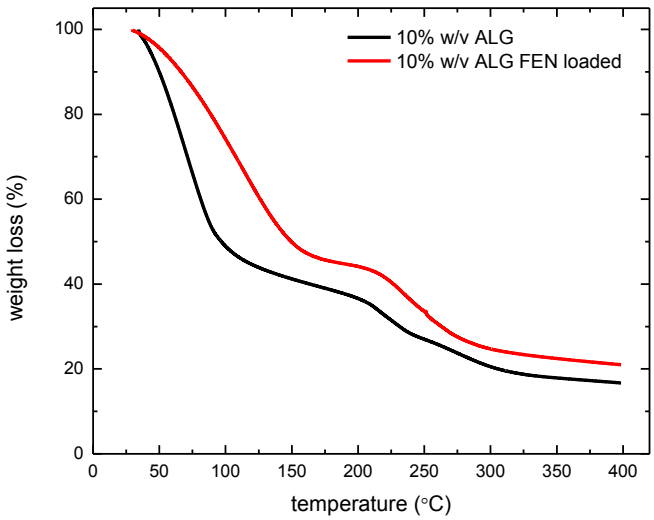


**Figure S8.** Thermographs of (a) 10% ALG particles in black, (b) 10% ALG particles loaded with FEN through nanoemulsification method in red.

TGA analysis showed that when hydrophobic drug FEN is encapsulated through HPH or magnetic stirrer emulsification (Figure S8), the residual solvent content is less when compared to the equilibrium partitioning method utilized for hydrophilic drug ACM (Figures S4-S7).

## IV. Nucleation induction time measurement.

The crystal nucleation induction time for the vials was monitored continuously with an inverted microscope in order to determine the average induction time of nucleation. Six different samples were prepared: bulk samples without ALG particles and samples with 5-10 ALG particles at different percent composition (4, 6, 8, 10, and 12%). For each type of samples 13 vials were prepared and loaded onto the temperature controlled block. The heating and cooling procedures were repeated to provide statistically

significant data for 78 samples. The samples were crash cooled from 65°C to 10°C to achieve a 1.5x supersaturated solution. The onset of each crystallization event was detected optically; when the first crystal was observed the frame number was recorded. Frames were taken at 5 min intervals. The average nucleation induction time, $\tau$, was determined from a statistical analysis of the induction time data, based on the knowledge that nucleation follows a Poisson distribution, $P(t) = e^{(-t/\tau)}$, where $P$ is the probability that no nucleation event occurs within time $t$[6].

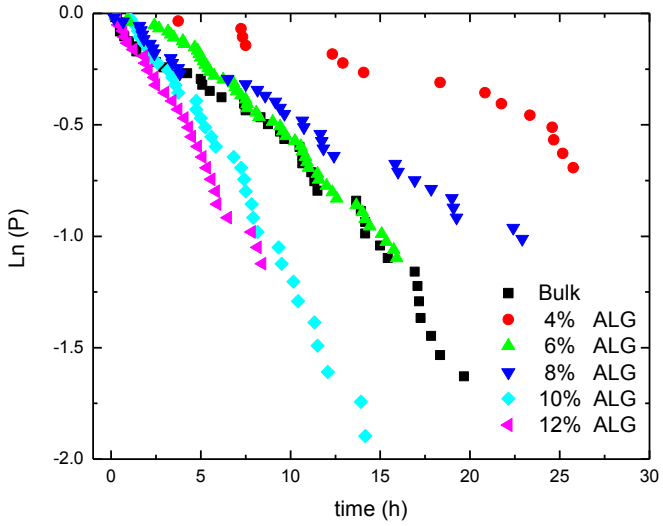


**Figure S9.** Time as a function of the natural logarithm of the nucleation induction probability for crystallizations in the presence of ALG particles at different percent composition (4%, 6%, 8%, 10%, and 12%) and the absence of ALG particles.

We think the ACM within hydrogels are in equilibrium with the ACM in the surrounding liquid despite the hindered diffusion. The diffusion coefficient of ACM in ALG gels have been previously measured by Julian et al[6] and Inoune[7] for various ALG concentrations. As expected it is lower than the bulk diffusion coefficient of ACM. For instance, the diffusion coefficient for 4% w/w ALG hydrogel is estimated as 1.8 $10^{-5}$ cm2/s. Using this value we can approximately calculate the time required for ACM to diffuse to the center of ALG beads. This characteristic time ($t_d$) is given below where $R_p$ is the radius of the hydrogel and DACM is the diffusion coefficient of ACM through the hydrogel.

$$\tau_d = \frac{R_p^2}{D_{ACM}}$$

This characteristic time is around 68s indicating that the ALG hydrogels come into equilibrium within mins. This diffusion time scale is dramatically shorter compared to induction time (order of hours depending on ALG concentration). This difference in time scales indicates that the time required for hydrogels to come to equilibrium is very short compared to induction time. Therefore, we reason that the kinetic effects are negligible.

## V. Direct compression into tablets.

About 250 mg of 10% w/v ALG particles loaded with ACM were pressed directly into a tablet in order to decrease water (solvent content). A 6mm mold was used in this study. The 10% w/v ALG particles loaded with ACM were compressed once with 500 Kg force inside a table maker. The resulting tablet is shown in Figure S10.

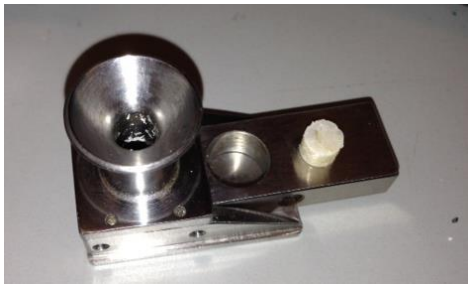

**Figure S10.** Image of the resulting tablet after direct compression of 10% w/v ALG particles loaded with ACM.

## VI. Encapsulation efficiency of FEN in emulsion-laden hydrogels

The encapsulation efficiency is dictated by the partitioning coefficient of FEN between the dispersed phase and the continuous phase –crosslinked alginate hydrogel, surfactant and the surrounding water. The hydrophobic nature of EA and HEP creates a favorable environment for FEN however FEN can escape from emulsions into surrounding aqueous phase. The solubility of FEN in EA and HEP are 600 mg/mL and 9 mg/mL respectively whereas solubility of FEN in the continuous phase containing aqueous solution of alginate and surfactant is 0.25 mg/ml. Hence we expect partitioning coefficients favoring the organic solvent. We believe only a small fraction of FEN can escape from the emulsion droplets into the aqueous phase.

To quantitatively determine the partitioning coefficient of FEN in hydrogel beads, we devised the following measurement. We added 10 mg of emulsion-laden hydrogels with the following formulation

(40% HEP/FEN in 4%ALG) into 50 ml of the continuous phase (%5 F68 in water). Then we have allowed the system to come to equilibrium overnight at room temperature. While stirring at 100 rpm, we measured the amount of FEN dissolved in water surrounding hydrogels using UV-vis at 290 nm. The concentration of FEN was calculated from Figure S11 as 10.2 μg/ml. As the initial concentration of FEN in dispersed phase is known i.e. 9 mg/ml, the partitioning coefficient is calculated as 889.35. This gives an encapsulation efficiency of 99.8%.

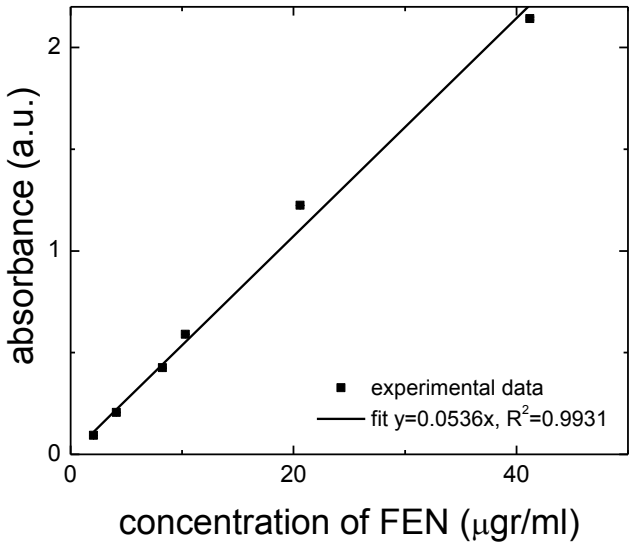


Figure S11 UV-Vis calibration curve of FEN in Ethanol.

## VII. References.


1. Strand, B. L.; Morch, Y. A.; Skjak-Braek, G., Alginate as immobilization matrix for cells. *Minerva Biotecnologica* **2000,** 12, (4), 223-233.
2. Turco, G.; Donati, I.; Grassi, M.; Marchioli, G.; Lapasin, R.; Paoletti, S., Mechanical Spectroscopy and Relaxometry on Alginate Hydrogels: A Comparative Analysis for Structural Characterization and Network Mesh Size Determination. *Biomacromolecules* **2011,** 12, (4), 1272-1282.
3. Augst, A. D.; Kong, H. J.; Mooney, D. J., Alginate hydrogels as biomaterials. *Macromolecular Bioscience* **2006,** 6, (8), 623-633.
4. Flory, P. J., *Principles of Polymer Chemistry*. Oxford University

Press: Ithaca,NY, 1953.
5. Gardel, M. L.; Shin, J. H.; MacKintosh, F. C.; Mahadevan, L.; Matsudaira, P.; Weitz, D. A., Elastic Behavior of cross-linked and bundled actin networks. *Science* **2004,** 304, (5675), 1301-1305.
6. Julian, T. N.; Radebaugh, G. W.; Wisniewski, S. J., Permeability Characteristics of Calcium Alginate Films. *Journal of Controlled Release* **1988,** 7, (2), 165-169.
7. Inoue, T.; Chen, G. H.; Hoffman, A. S.; Nakamae, K., A hydrophobically modified bioadhesive polymeric carrier for controlled drug delivery to mucosal surfaces. *Journal of Bioactive and Compatible Polymers* **1998,** 13, (1), 50-64.